

CHAPTER ONE HUNDRED NINETY SIX

ATTENUATION OF WAVE INDUCED OSCILLATION IN PORTS BY IMPROVING THE CONDITIONS AT THE HARBOR ENTRANCE

M. Kubo¹, S. Aoki² and J.J. Avitia Segura³

ABSTRACT

The authors developed the numerical method to calculate the wave height distribution around a pair of breakwaters with arbitrary shape of the edge. The effect of the resonators equipped in the breakwaters on the diffracted wave height is simulated by using this method. Simulated results show that the resonators have remarkable effect to reduce wave heights in a harbor. However, in the experiments, resonators are not so effective as predicted by the theory.

I. INTRODUCTION

A harbor should be a protected zone of water, able to bring safety for ships to permit the activities of traffic of merchandises and persons at all time. However, in harbors suffering from storm waves, cargo handlings are often interrupted and sometimes mooring lines are broken by large ship motions.

In order to protect a harbor from waves, a lot of money have been spent in constructing breakwaters. No matter how effective breakwater may be, waves pass through the breakwater gap inevitably. Once waves enter the harbor, it is difficult to absorb these energy in the harbor surrounded with vertical walls, and sometimes harbor resonance is induced when the wave period is close to the natural period of the harbor.

So the development of a new method to trap the wave energy before the waves enter the harbor is desired. As a new method to trap the wave energy, a resonator was introduced by Valembos in 1953 and defined as a wave absorber which can trap the wave energy by taking advantage of the resonance phenomenon. After that, some researchers investigated the wave resonators built in a channel and showed that they were sufficiently effective. (for example, W. James (1968,1970))

In this paper, we deal with diffraction problem by the breakwaters equipped with a resonator. The mathematical model is proposed to predict the diffracted wave height distribution for arbitrary shape of entrance and for any angle of the wave incidence. By using this

-
1. Associate Professor, Kobe Univ. of Mercantile Marine, Kobe, Japan
 2. Research Associate, Osaka Univ., Osaka, Japan
 3. Planeacion y Proyectos S.C., Mexico

model, wave transformation around the wave resonators is simulated. The calculated wave height are discussed by comparing with the experimental results.

II. THEORY AND NUMERICAL PROCEDURE

In this section, first, the theoretical analysis to predict the diffracted wave height distribution for arbitrary shape of entrance is developed by modifying Lee's method (1970) which is widely used to calculate the wave height distribution in a harbor. Then, the numerical procedure to simulate diffracted waves are shown. Finally, the procedure is verified by comparing with the analytical solutions.

(A) Theory

Let us take z axis upward from the still water level and assume that the fluid is invicid and the motion is irrotational. The equation of continuity for an incompressible fluid is expressed by the Laplace equation by using the velocity potential $\Phi(x,y,z,t)$:

$$\frac{\partial^2 \Phi}{\partial x^2} + \frac{\partial^2 \Phi}{\partial y^2} + \frac{\partial^2 \Phi}{\partial z^2} = 0 \quad (1)$$

For a sinusoidal wave with frequency ω , Φ which satisfies the boundary condition at $z=-h$, $\partial \Phi / \partial z = 0$ is expressed as

$$\Phi(x,y,z,t) = A \frac{\cosh k(h+z)}{\cosh kh} f(x,y) e^{-i\omega t} \quad (2)$$

where A : constant,
 h : constant water depth,
 k : wave number,
 $\omega = \sqrt{-1}$,

and $f(x,y)$ is the wave function which satisfies the Helmholtz equation:

$$\frac{\partial^2 f(x,y)}{\partial x^2} + \frac{\partial^2 f(x,y)}{\partial y^2} + k^2 f(x,y) = 0 \quad (3)$$

The velocity potential of the fluid motion is determined by solving Eq. (3) under boundary conditions.

Fig. 1 shows a pair of straight breakwaters with arbitrary shape of edges and a coordinate system. To solve Eq.(3) in the domain of interest shown in Fig.1, we divide it into three regions. I is the open sea region, II is the entrance region and III is the harbor region. The velocity potential in each region is described as Φ_I , Φ_{II} and Φ_{III} . Φ_I can be divided into two terms Φ_{I0} and Φ_{I1} and described as follows:

$$\Phi_I = \Phi_{I0} + \Phi_{I1} = A \frac{\cosh k(h+z)}{\cosh kh} (f_0 + f_1) e^{-i\omega t} \quad (4)$$

where suffix 0 represents the composite waves of the incident and reflected waves when the boundary C_1 is closed, and suffix 1 indicates the quantities concerning with the correction term due to the scattering waves from the region II.

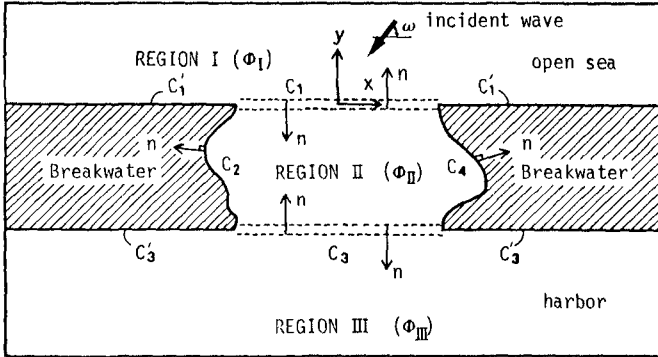


Fig.1 The domain of interest and the coordinate

If the incident wave profile ζ_I is given by the following equation:

$$\zeta_I = \zeta_0 \exp \{ -i (k_x x \cos \omega + k_y y \sin \omega + \omega t) \}, \tag{5}$$

the surface profile of the composite waves $\zeta_I + \zeta_R$ becomes

$$\zeta_I + \zeta_R = 2 \zeta_0 \cos(k_y y \sin \omega) e^{-i k_x x \cos \omega} \cdot e^{-i \omega t} \tag{6}$$

where ζ_0 is the amplitude of the incident waves and ω is the angle of the wave incidence defined in Fig.1. Another description of the surface profile is given by the dynamic condition on the free surface.

$$\zeta_I + \zeta_R = -\frac{1}{g} \left(\frac{\partial \Phi_{I0}}{\partial t} \right)_{z=0} = \frac{i \omega}{g} A f_0 e^{-i \omega t} \tag{7}$$

Comparing Eq.(6) and Eq.(7) and taking $A = \frac{g \zeta_0}{i \omega}$, Φ_I is expressed by

$$\Phi_I = \frac{g \zeta_0}{i \omega} \frac{\cosh k(h+z)}{\cosh k h} (f_0 + f_1) e^{-i \omega t} \tag{8}$$

where

$$f_0 = z \cos(k_y y \sin \omega) e^{-i k_x x \cos \omega} \tag{9}$$

Similarly the velocity potentials in region II and III can be expressed as

$$\Phi_{II} = \frac{g\zeta_0}{\lambda\sigma} \cdot \frac{\cosh k(R+kz)}{\cosh kR} f_2 e^{-i\omega t} \quad (10)$$

$$\Phi_{III} = \frac{g\zeta_0}{\lambda\sigma} \cdot \frac{\cosh k(R+kz)}{\cosh kR} f_3 e^{-i\omega t} \quad (11)$$

Taking the normal vector n of each region outward, the conditions of continuity of pressure and velocity between each region are described as follows:

on C_1

$$f_0 + f_1 = f_2 \quad (12)$$

$$\frac{\partial f_1}{\partial n} = -\frac{\partial f_2}{\partial n} \quad (\because \frac{\partial f_0}{\partial n} = 0) \quad (13)$$

on C'_1

$$\frac{\partial f_1}{\partial n} = 0 \quad (\because \frac{\partial f_0}{\partial n} = 0) \quad (14)$$

on C_2, C_4

$$\frac{\partial f_2}{\partial n} = 0 \quad (15)$$

on C_3

$$f_2 = f_3 \quad (16)$$

$$\frac{\partial f_2}{\partial n} = -\frac{\partial f_3}{\partial n} \quad (17)$$

on C'_3

$$\frac{\partial f_3}{\partial n} = 0 \quad (18)$$

Furthermore the radiation condition must be considered:

$$f_i \rightarrow 0, \quad f_3 \rightarrow 0 \quad ; \quad \text{when } \sqrt{x^2+y^2} \rightarrow \infty \quad (19)$$

While, the wave function f_i ($i=1,2,3$) at any position inside each region can be expressed in terms of f_i and $\frac{\partial f_i}{\partial n}$ at the boundary of each region by applying Weber's solution of Helmholtz equation and Eq.(19).

$$f_1 = -\frac{\lambda}{4} \int_{C_1+C'_1} \left\{ f_1 \frac{\partial}{\partial n} H_0^{(1)}(kR) - H_0^{(1)}(kR) \frac{\partial f_1}{\partial n} \right\} ds \quad (20)$$

$$f_2 = -\frac{\lambda}{4} \int_{C_1+C_2+C_3+C_4} \left\{ f_2 \frac{\partial}{\partial n} H_0^{(1)}(kR) - H_0^{(1)}(kR) \frac{\partial f_2}{\partial n} \right\} ds \quad (21)$$

$$f_3 = -\frac{\lambda}{4} \int_{C_3+C'_3} \left\{ f_3 \frac{\partial}{\partial n} H_0^{(1)}(kR) - H_0^{(1)}(kR) \frac{\partial f_3}{\partial n} \right\} ds \quad (22)$$

,where $H_0^{(1)}(kr)$ is the zeroth order Hankel function of the first kind and r is the distance between the point inside the region and that on the boundary. Similarly, f_i on the boundary is expressed in terms of f_i and $\partial f_i / \partial n$ on the boundary as follows:

$$\begin{aligned}
 f_1(\text{on } C_1, C_1') &= -\frac{i}{2} \int_{C_1+C_1'} \left\{ f_1 \frac{\partial}{\partial n} H_0^{(1)}(kr) - H_0^{(1)}(kr) \frac{\partial f_1}{\partial n} \right\} ds \\
 &= -\frac{i}{2} \int_{C_1} H_0^{(1)}(kr) \frac{\partial f_1}{\partial n} ds \quad (23) \\
 (\because \partial f_1 / \partial n &= 0 \text{ on } C_1 \text{ and } \frac{\partial}{\partial n} H_0^{(1)}(kr) = 0 \text{ on } C_1 \text{ and } C_1')
 \end{aligned}$$

$$f_2(\text{on } C_1, C_2, C_3, C_4) = -\frac{i}{2} \int_{C_1+C_2+C_3+C_4} \left\{ f_2 \frac{\partial}{\partial n} H_0^{(1)}(kr) - H_0^{(1)}(kr) \frac{\partial f_2}{\partial n} \right\} ds \quad (24)$$

$$\begin{aligned}
 f_3(\text{on } C_3, C_3') &= -\frac{i}{2} \int_{C_3+C_3'} \left\{ f_3 \frac{\partial}{\partial n} H_0^{(1)}(kr) - H_0^{(1)}(kr) \frac{\partial f_3}{\partial n} \right\} ds \\
 &= -\frac{i}{2} \int_{C_3} H_0^{(1)}(kr) \frac{\partial f_3}{\partial n} ds \quad (25)
 \end{aligned}$$

Using Eqs. (12), (13) and (23),

$$f_2 = f_0 - \frac{i}{2} \int_{C_1} H_0^{(1)}(kr) \frac{\partial f_2}{\partial n} ds \quad (\text{on } C_1) \quad (26)$$

Eqs. (15) and (24) give the relation

$$f_2 = -\frac{i}{2} \int_{C_1+C_2+C_3+C_4} f_2 \frac{\partial}{\partial n} H_0^{(1)}(kr) ds + \frac{i}{2} \int_{C_1+C_3} H_0^{(1)}(kr) \frac{\partial f_2}{\partial n} ds \quad (\text{on } C_1+C_2+C_3+C_4) \quad (27)$$

and Eqs. (16), (17) and (25) lead to the equation

$$f_2 = -\frac{i}{2} \int_{C_3} H_0^{(1)}(kr) \frac{\partial f_2}{\partial n} ds \quad (\text{on } C_3) \quad (28)$$

The wave function f_2 and $\partial f_2 / \partial n$ are determined by solving Eqs. (26), (27) and (28). While, Eqs. (20) and (22) can be rewritten as follows, by using Eqs. (12), (13), (16) and (17):

$$\begin{aligned}
 f_1 &= -\frac{i}{4} \int_{C_1} \left\{ f_2 \frac{\partial}{\partial n} H_0^{(1)}(kr) + H_0^{(1)}(kr) \frac{\partial f_1}{\partial n} \right\} ds \\
 &\quad - \frac{i}{4} \int_{C_1'} f_1 \frac{\partial}{\partial n} H_0^{(1)}(kr) ds \quad (29)
 \end{aligned}$$

$$\begin{aligned}
 f_3 &= -\frac{i}{4} \int_{C_3} \left\{ f_2 \frac{\partial}{\partial n} H_0^{(1)}(kr) + H_0^{(1)}(kr) \frac{\partial f_3}{\partial n} \right\} ds \\
 &\quad - \frac{i}{4} \int_{C_3'} f_3 \frac{\partial}{\partial n} H_0^{(1)}(kr) ds \quad (30)
 \end{aligned}$$

In these equations, f_1 on C'_1 and f_3 on C'_3 are given by substituting Eqs. (13) and (17) into Eqs. (23) and (25):

$$f_1 = -\frac{\lambda}{2} \int_{C_1} H_0^{(1)}(kr) \frac{\partial f_2}{\partial n} ds \quad (\text{on } C'_1) \quad (31)$$

$$f_3 = -\frac{\lambda}{2} \int_{C_3} H_0^{(1)}(kr) \frac{\partial f_2}{\partial n} ds \quad (\text{on } C'_3) \quad (32)$$

Consequently, f_1 and f_3 inside each region are expressed in terms of f_2 and $\frac{\partial f_2}{\partial n}$ on the boundary as follows:

$$f_1 = -\frac{\lambda}{4} \int_{C_1} \left\{ f_2 \frac{\partial}{\partial n} H_0^{(1)}(kr) + H_0^{(1)}(kr) \frac{\partial f_2}{\partial n} \right\} ds - \frac{\lambda}{4} \int_{C'_1} \left\{ -\frac{\lambda}{2} \int_{C_1} H_0^{(1)}(kr) \frac{\partial f_2}{\partial n} ds \right\} \frac{\partial}{\partial n} H_0^{(1)}(kr) ds \quad (33)$$

$$f_3 = -\frac{\lambda}{4} \int_{C_3} \left\{ f_2 \frac{\partial}{\partial n} H_0^{(1)}(kr) + H_0^{(1)}(kr) \frac{\partial f_2}{\partial n} \right\} ds - \frac{\lambda}{4} \int_{C'_3} \left\{ -\frac{\lambda}{2} \int_{C_3} H_0^{(1)}(kr) \frac{\partial f_2}{\partial n} ds \right\} \frac{\partial}{\partial n} H_0^{(1)}(kr) ds \quad (34)$$

Finally, the variations of the free surface in each region are given as follows:

$$\zeta_1 = -\frac{1}{g} \left(\frac{\partial \Phi_I}{\partial t} \right)_{z=0} = \zeta_0 (f_0 + f_1) e^{-\lambda \alpha t} \quad (35)$$

$$\zeta_2 = -\frac{1}{g} \left(\frac{\partial \Phi_{II}}{\partial t} \right)_{z=0} = \zeta_0 f_2 e^{-\lambda \alpha t} \quad (36)$$

$$\zeta_3 = -\frac{1}{g} \left(\frac{\partial \Phi_{III}}{\partial t} \right)_{z=0} = \zeta_0 f_3 e^{-\lambda \alpha t} \quad (37)$$

Therefore, the diffraction coefficient K_d is determined by

$$K_d = \left| \frac{\zeta_3}{\zeta_2} \right| = \left| \frac{\zeta_0 f_3 e^{-\lambda \alpha t}}{\zeta_0 f_2 e^{-\lambda (\kappa x \cos \omega + \kappa y \sin \omega) t} e^{-\lambda \alpha t}} \right| = \left| f_3 \right| \quad (38)$$

(C) Numerical Procedure

In order to solve Eqs. (26), (27) and (28) numerically, we divided the boundaries into some segments as shown in Fig.2, and then these equations are described in discrete form at each segment as follows:

$$f_2(\lambda) = f_0(\lambda) - \frac{\lambda}{2} \sum_{j=1}^{N_1} H_0^{(1)}(\kappa r_{\lambda j}) \bar{f}_2(j) \Delta S_j \quad (\lambda=1, N_1) \quad (39)$$

$$f_2(\lambda) = \frac{i}{2} R \sum_{j=1}^{N_1+N_2+N_3+N_4} f_2(j) H_1^{(1)}(Rr_{\lambda j}) \Delta s_j - \frac{i}{2} R \sum_{j=1}^{N_1+N_3} H_0^{(1)}(Rr_{\lambda j}) \bar{f}_2(j) \Delta s_j \quad (\lambda=1, N_1+N_2+N_3+N_4) \quad (40)$$

$$f_2(\lambda) = -\frac{i}{2} R \sum_{j=1}^{N_3} H_0^{(1)}(Rr_{\lambda j}) \bar{f}_2(j) \Delta s_j \quad (\lambda=1, N_3) \quad (41)$$

where $\bar{f}_2(j) = \frac{1}{R} \frac{\partial f_2(j)}{\partial n}$, $H_0^{(1)}(Rr_{\lambda j})$ is the first order Hankel function of the first kind, i and j are the calculation points on the boundary.

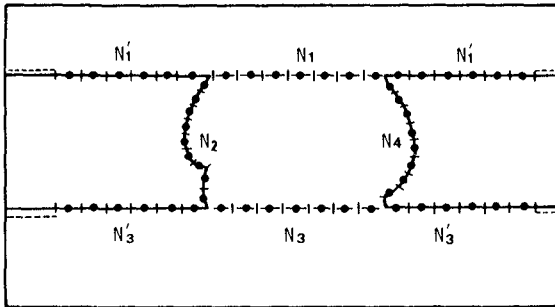


Fig.2 Segmentation of boundaries

The number of unknowns f_2 and \bar{f}_2 is $2N_1+N_2+2N_3+N_4$ and the number of equations is the same. So, f_2 and \bar{f}_2 on the boundaries C_1, C_2, C_3 and C_4 are given by solving Eqs. (39), (40) and (41).

Eqs. (33) and (34) are also rewritten as follows:

$$f_1(x, y) = -\frac{i}{4} R \sum_{j=1}^{N_1} \{ f_2(j) H_1^{(1)}(Rr_{xj}) + H_0^{(1)}(Rr_{xj}) \bar{f}_2 \} \Delta s_j - \frac{i}{4} R \sum_{j=1}^{2N_1} \{ -\frac{i}{2} R \sum_{\ell=1}^{N_1} H_0^{(1)}(Rr_{j\ell}) \bar{f}_2(\ell) \Delta s_\ell \} H_1^{(1)}(Rr_{xj}) \Delta s_j \quad (42)$$

$$f_3(x, y) = -\frac{i}{4} R \sum_{j=1}^{N_3} \{ f_2(j) H_1^{(1)}(Rr_{xj}) + H_0^{(1)}(Rr_{xj}) \bar{f}_2 \} \Delta s_j - \frac{i}{4} R \sum_{j=1}^{2N_3} \{ -\frac{i}{2} R \sum_{\ell=1}^{N_3} H_0^{(1)}(Rr_{j\ell}) \bar{f}_2(\ell) \Delta s_\ell \} H_1^{(1)}(Rr_{xj}) \Delta s_j \quad (43)$$

Although the number of segments N_1' and N_3' must be infinite, we put them finite because the influence of the point far away from the region II is very small. Here, the length of C_1' and C_3' is taken 10 times of wave length.

(c) Verification of numerical solution

Here, the validity of the numerical method and the stability of the solution are discussed. Fig.3 shows a pair of breakwaters with square edge. For this type of breakwaters, some analytical solutions of diffraction were obtained. However, there is the limitation in these solutions that the width of a breakwater is infinitely small. So, the numerical solutions used in this study are compared with the analytical solutions proposed by Takayama (1981) for the case of small width of a breakwater.

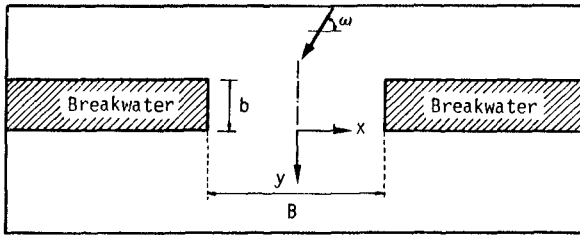


Fig.3 A pair of straight breakwaters with square edges

Figs. 4 (a) to (d) show the diffraction coefficient K_d at the point of $Y/L=0.1, 0.5$ and 1.0 for the case of $b/L=0.01, B/L=0.5$ and $\omega = 90^\circ, 150^\circ$ and 165° . In these cases, the maximum length of a segment $D_{max} \leq L/10$ (L : wave length), namely, each boundary is divided into small segments whose length is smaller than $L/10$.

As can be seen from these figures, the solutions of the proposed numerical method (shown by the broken lines) are a little smaller than the exact solutions shown by the solid lines. These small differences are not improved by shortening the length of a segment. It is not clear whether these differences come from the influence of the width of a breakwater or from the numerical error. However, the results of our numerical method sufficiently agree with the analytical solutions.

Next we calculated the wave height distribution for rectangular resonators shown in Fig.5. Fig.6 shows the diffraction coefficient K_d with wave resonators at the point of $X/B=0.0$ and $Y/B=1.33$ and the amplification factor ζ_A/ζ_I for the case of $L/B=0.5, B_R/B=0.08$ and $b_R/B=0.03$. The solid lines represent the case where the maximum length of a segment D_{max} is smaller than $L/20$ and the broken lines represent the case of $D_{max} \leq L/50$.

It is noted that the difference between two curves is remarkable especially near the resonant point in the resonator. It is also found that it is impossible to stabilize the numerical solution even in the case of $D_{max} \leq L/100$ when the resonance takes place. The reason for this unstability is supposed that the value of a calculation point does not correspond to the value on a segment owing to the marked variation of f_z and $\partial^2 \zeta_2 / \partial n^2$ in the resonators. So it is difficult to obtain stable solutions (especially in the state of resonance) even if

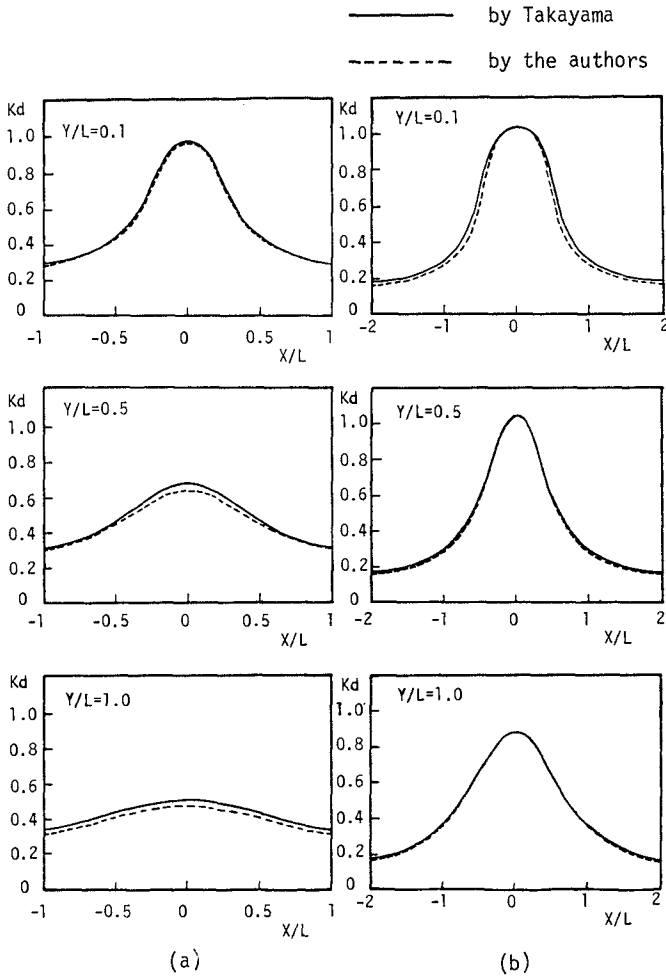


Fig.4 Diffraction coefficients K_d

(a) $\omega=90^\circ$, $B/L=0.5$, $b/L=0.01$, $D_{max}/L=0.08$

(b) $\omega=90^\circ$, $B/L=1.0$, $b/L=0.01$, $D_{max}/L=0.09$

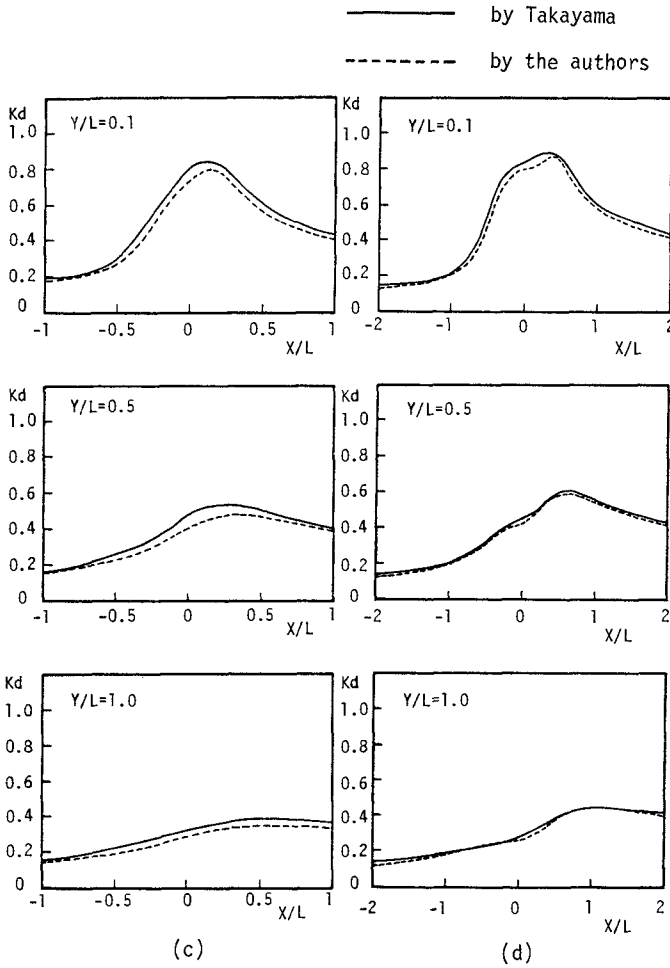


Fig.4 Diffraction coefficients K_d
 (c) $\omega = 150^\circ$, $B/L = 0.5$, $b/L = 0.01$, $D_{max}/L = 0.08$
 (d) $\omega = 165^\circ$, $B/L = 1.0$, $b/L = 0.01$, $D_{max}/L = 0.09$

the length of the segment is considerably small. However, judging from the results shown in Fig.6, it is reasonable to consider that our numerical method is applicable to discuss the variation of diffraction coefficients qualitatively because the variation of K_d with varying L/B calculated from different D_{max} are similar.

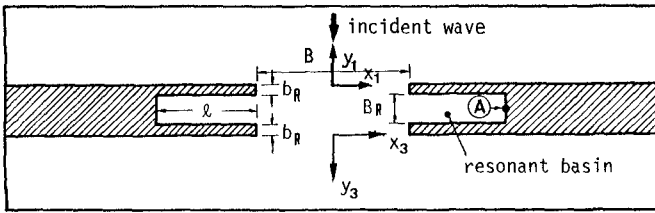


Fig.5 Wave resonators in breakwaters and the coordinates

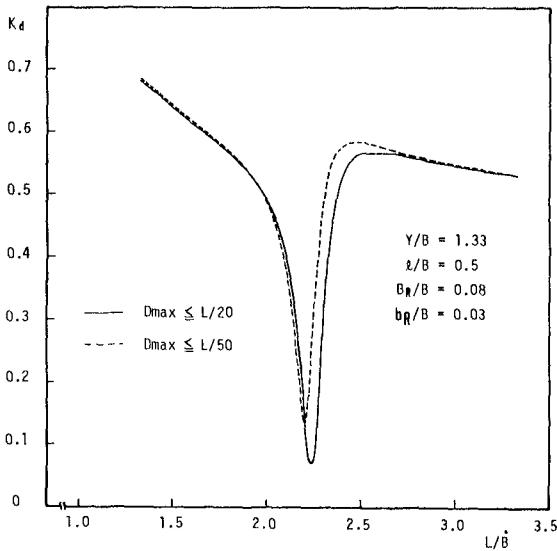


Fig.6-(a) Variations of diffraction coefficient K_d with wave resonators

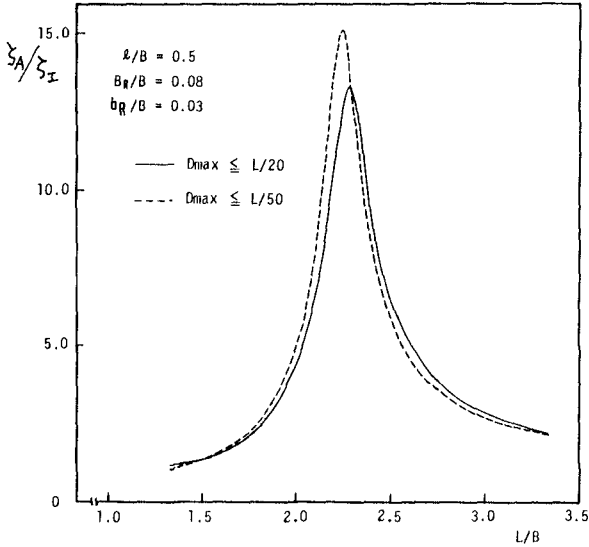


Fig.6-(b) Amplification factor ζ_A/ζ_I at the point of (A)

III. THEORETICAL DEFINITION AND EFFECTS OF A WAVE RESONATOR

As shown in Fig.6, the diffraction coefficients in the case with resonators are strongly dependent on the wave length (i.e. wave period) and indicate a remarkable decrease at the point where the resonance occurs in the resonators ($L/B = 2.2$). In this section, the function of a wave resonator that diminishes the diffracted wave height is investigated theoretically.

Firstly, let us divide f_1 and f_3 in Eqs.(8) and (11) into two components respectively:

$$f_1 = f_{10} + f_{1R} \tag{44}$$

$$f_3 = f_{30} + f_{3R} \tag{45}$$

where f_{10} and f_{30} are the wave function in the case without resonator and f_{1R} and f_{3R} represent the influence of resonators on f_1 and f_3 and are called here after the wave functions of radiated waves from resonators. f_{1R} and f_{3R} are obtained by calculating f_1 , f_3 , f_{10} and f_{30} .

Fig.7 and Fig.8 illustrate the wave height distribution in region I and III when $\omega=90^\circ$. Fig.(a) in each figures shows the wave height distribution around breakwaters without resonators, Fig.(b) represents the radiated waves from resonators obtained by using Eqs.(44) and (45) and Fig.(c) shows the wave height distribution in the case with resonators. The wave height distribution in Fig.(c) can be regarded as the composite waves of the diffracted waves in Fig.(a) and the radiated waves in Fig.(b). The numerals in these figures indicate the ratio of the wave height to the incident wave height H/H_1 .

The geometric profile and dimensions of the resonator in Figs. 7 and 8 corresponds to that in Fig.6. Fig.7 shows the wave height distributions in the case of $L/B=2.5$. In this case, the amplification factor at the point A in the resonator ζ_A/ζ_1 is small as shown in Fig.6 (b). Fig.8 shows the wave height distribution in the case of $L/B=2.2$ and it is found from Fig.6 (b) that the resonance occurs in the resonators.

In the case of Fig.7, the radiated wave height is relatively small. Therefore the difference of the wave height distribution in Fig.(c) is similar to that in Fig.(a). On the other hand, in the case of Fig.8, the composite wave height in the harbor region becomes very small, and at the same time, the radiated wave height shown in Fig.8(b) is much larger than Fig.7-(b). The distribution of the radiated waves in the harbor (Fig.8-(b)) is similar to that of diffracted waves without resonators shown in Fig.8-(a).

So it is clear that the effectiveness of resonators comes from the phase interaction between diffracted waves in the case without resonator and the radiated waves from resonators. However, it must be paid attention to the fact that the wave heights in the open sea region becomes larger than those in the case without resonator. (See Fig.8-(c))

Fig.9 and Fig.10 show the wave height distribution in the case where resonance takes place when the entrance width B is larger than the wave length L . These figures demonstrate that each resonator located at the edge of breakwater has a tendency to function independently as the ratio L/B becomes small. The wave height distribution is much different from that shown in Fig.8 and the resonators is not so effective to reduce the diffracted wave height.

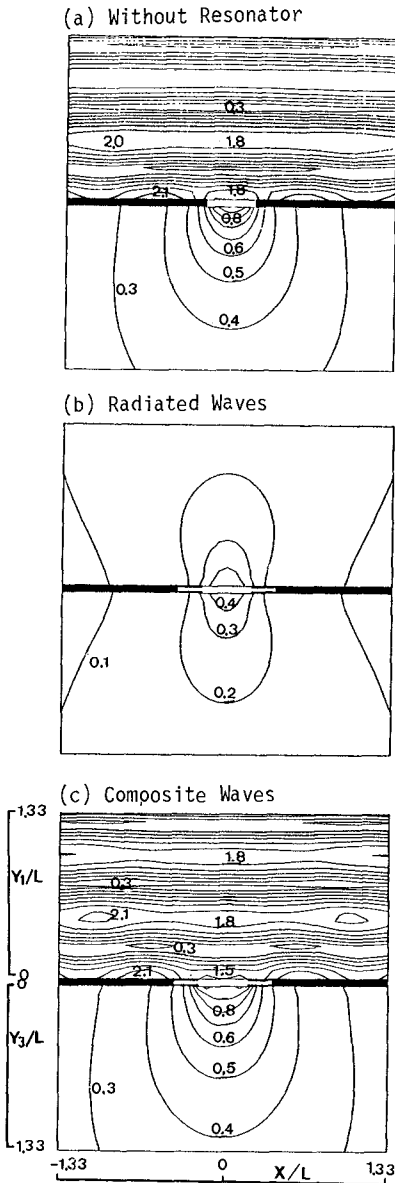


Fig.7 Wave height distribution
($L/B=2.5, B/B=0.5, B/B=0.08, b/B=0.03$)

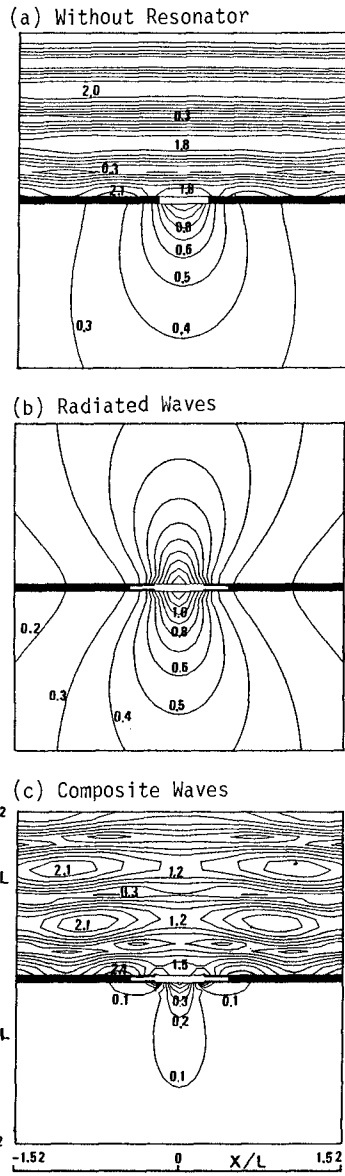
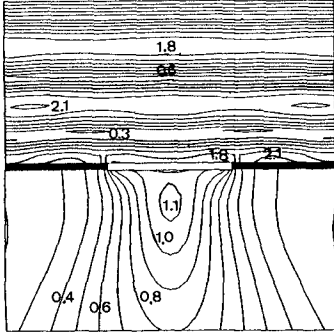
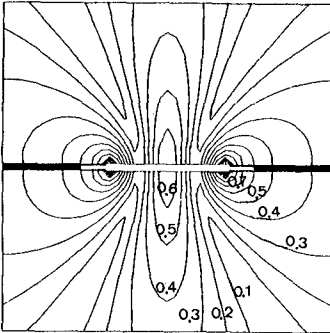


Fig.8 Wave height distribution
($L/B=2.2, B/B=0.5, B/B=0.08, b/B=0.03$)

(a) Without Resonator



(b) Radiated Waves



(c) Composite Waves

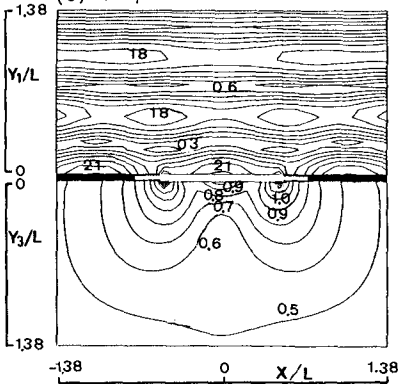
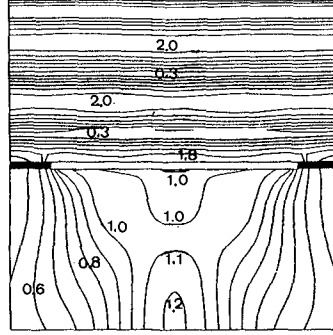
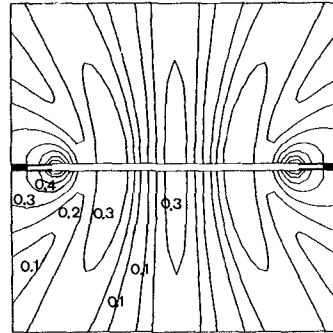


Fig.9 Wave height distribution
($L/B=0.97$, $/B=0.2$, $B/B=0.03$, $b/B=0.013$)

(a) Without Resonator



(b) Radiated Waves



(c) Composite Waves

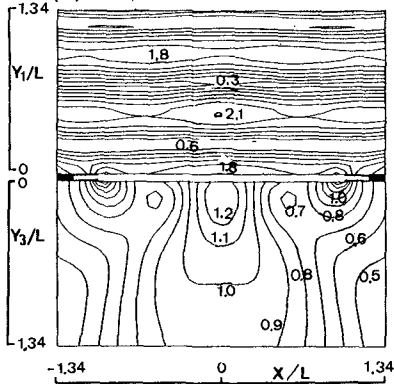


Fig.10 Wave height distribution
($L/B=0.5$, $/B=0.1$, $B/B=0.015$, $b/B=0.007$)

IV. EXPERIMENTAL VERIFICATION

Judging from the numerical calculation, resonators are very effective to diminish the diffracted wave height and are expected to reduce harbor oscillation. In order to verify these results, model tests were carried out in a wave basin of 15m x 5m and 0.6m deep shown in Fig.11.

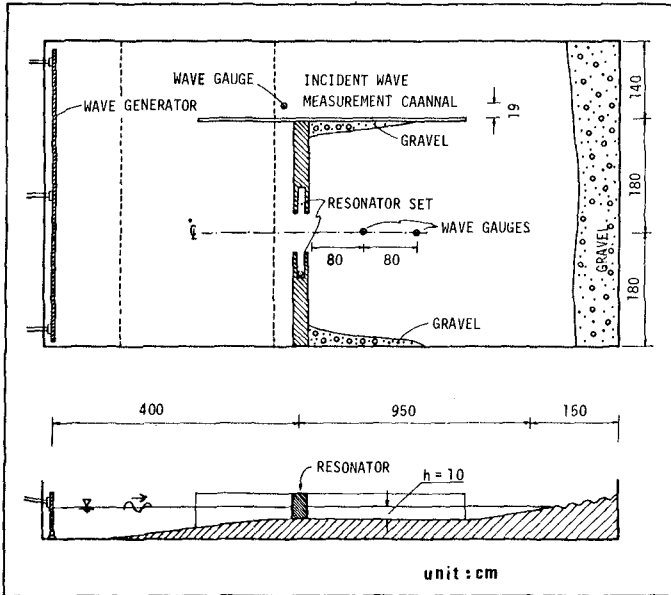


Fig.11 Wave basin

In the wave basin, an over floor made of wood was constructed in order to generate waves of about 2cm height at the depth of 10cm. A flap type wave generator located at one end of the basin was used. At the other end, a gravel sloped beach was equipped as a wave absorber. A lateral wave channel to measure the incident waves during the experiments was also prepared.

Three types of resonators (Case-A, Case-B and Case-C) shown in Fig. 12 (a), (b) and (c) were tested. The results obtained in these cases are shown in Fig.13, 14 and 15 by comparing with theoretical results. The theoretical results in the case C was calculated by using Lee's method.

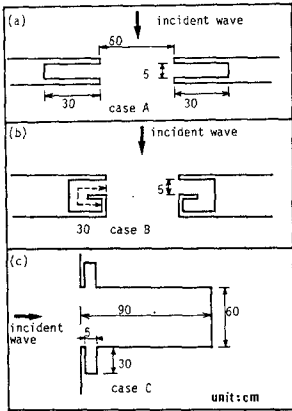


Fig. 12 Experimental cases

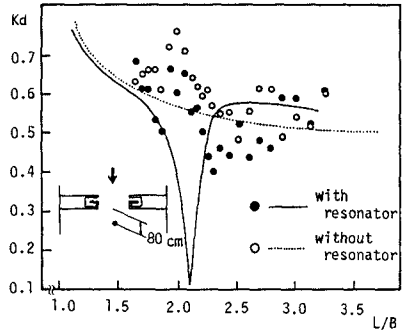


Fig. 14 Diffraction coefficient (Case-B)

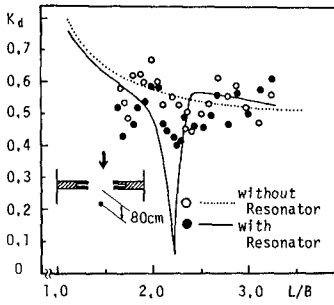


Fig. 13 Diffraction coefficient (Case-A)

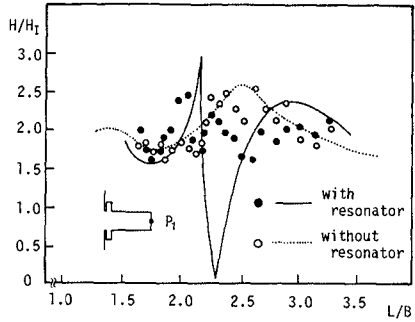


Fig. 15 Amplification factor at P_1 (Case-C)

In all these cases, the abscissas represent the ratio of the wave length to the width of the harbor entrance L/B . The ordinates in Figs. 13 and 14 are the diffraction coefficient K_d at the point of 80cm away from the breakwaters in the harbor region. The ordinate in Fig.15 shows the amplification factor at the point P_1 in Fig.15. The dotted lines represent the calculated response in the case without resonator and the open circles are the experimental results. The solid lines are the calculated response in the case with resonators and closed circles show the experimental results.

The calculated results indicate an apparent decrease of wave height when a resonance takes place in the resonator, but such a decrease can not be seen in all experiments as shown in Figs. 13 to 15. It is also found that the agreement between experimental results and theoretical ones is not good even in the case without resonator. The cause of this is assumed that the transversal oscillation in the wave basin exists. Of course, in the case where the resonator was equipped, this transversal oscillation also affected the experimental results. However, this is not the main reason why the experimental results do not show a significant decrease.

As mentioned above, only when the resonance occurs in the resonators the resonators become effective to reduce the diffracted wave height. So the response in the resonator was investigated based on the experimental results obtained in Case-A. Fig. 16 shows the amplification factor H/H_x at the point (A) in the resonator shown in Fig.5. Clearly, the resonance in the experiments is not as remarkable as that in the calculated results and the measured peak of the response appears at the different position from the calculated response. This is probably due to the energy dissipation at the resonator mouth.

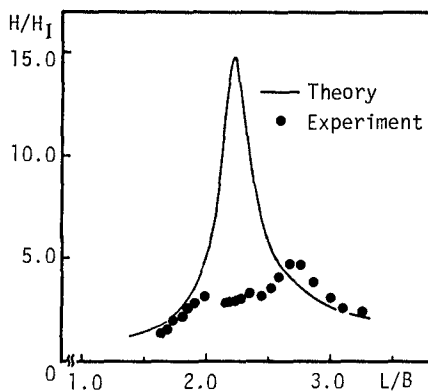


Fig.16 Amplification factor at (A) in the resonator (Case-A)

Consequently, it must be concluded that the wave resonators treated here are not so effective as predicted by the theory, and the reason is considered that sufficient resonance to reduce the diffracted wave height does not occur in the resonator.

V. CONCLUSIONS

In this paper, the effect of wave resonators on wave diffraction by breakwaters was investigated theoretically and experimentally. The numerical method developed here shows that resonators equipped at the edge of a breakwater are very effective to reduce diffracted wave heights when resonance occurs in resonators. This effect comes from the phase interaction between the diffracted waves in the case without resonator and the radiated waves from resonators.

The effectiveness of resonators predicted by the numerical simulation was not verified by experiments. The main reason of this is supposed to be the energy dissipation at the resonator mouth which prevents from occurring the sufficient resonance in the resonator.

REFERENCES

- James W. (1968) : Rectangular Resonators for Harbour Entrances, Proc. of 11th ICCE, Chapter 98
- James W. (1970) : Spectral Response of Harbor Resonator Configurations, Proc. of 12th ICCE, Chapter 132
- Lee J.J. and Raichlen F. (1970) : Resonance in Harbors of Arbitrary Shape, Proc. of 12th ICCE, Chapter 131
- Takayama T. (1981) : Wave Diffraction and Wave Height Distribution inside a Harbor, Doctral Thesis, Kyoto University
- Valembois J. (1953) : Etude de l'Action d'Ouvrages Resonants et leur Applicayion a la Protection de la Houle, Minnesota International Hydraulic Convention